Effects of rail dynamics and friction characteristics on curve squeal

B Ding, G Squicciarini and D J Thompson

Institute of Sound and Vibration Research, University of Southampton, University Road, Southampton SO17 1BJ, UK

Email: B.Ding@soton.ac.uk

Abstract. Curve squeal in railway vehicles is an instability mechanism that arises in tight curves under certain running and environmental conditions. In developing a model the most important elements are the characterisation of friction coupled with an accurate representation of the structural dynamics of the wheel. However, the role played by the dynamics of the rail is not fully understood and it is unclear whether this should be included in a model or whether it can be safely neglected. This paper makes use of previously developed time domain and frequency domain curve squeal models to assess whether the presence of the rail and the falling characteristics of the friction force can modify the instability mechanisms and the final response. For this purpose, the time-domain model has been updated to include the rail dynamics in terms of its state space representation in various directions. Frequency domain and time domain analyses results show that falling friction is not the only reason for squeal and rail dynamics can play an important role, especially under constant friction conditions.

1. Introduction

Railway curve squeal is a loud and often annoying tonal noise usually found in tight curves. Although it has been studied for decades, the mechanism behind this phenomenon is still controversial. Rudd [1] was the first to indicate that the wheel response was unstable due to the falling friction characteristics at large sliding velocities, which was described as negative damping that could feed energy into the system in each period of vibration. Rudd's work has been widely accepted and, following his work, many subsequent models that appeared in the literature adopt parts of Rudd's approach to the theoretical modelling of squeal [2-7]. However, another type of instability, called mode coupling, may also be able to induce curve squeal. To explain the mechanism of mode-coupling instability, Hoffmann *et al.* [8] used a two degree of freedom model to show that the constant friction force can lead to a non-symmetric stiffness matrix, and with increasing friction coefficient, to instability. As a consequence two structural modes originally with different natural frequencies converge and, when the two natural frequencies are equal, one of the two becomes unstable. This behaviour is also known in literature as flutter. Glocker *et al.* [9] and Pieringer [10] showed that curve squeal can exist with a constant friction coefficient according to this mechanism.

Besides the mechanism of curve squeal, the role played by the rail in curve squeal is also not fully understood. To explore the mechanism of curve squeal and the role of rail dynamics, in this paper the curve squeal model from Huang [11] is used and extended. In his model, a falling friction law was considered and a method introduced by Wu and Thompson [12] was used to represent rail dynamics in the time domain. This consisted in finding a low order equivalent system corresponding to each rail mobility curve, according to which the rail mobility in each direction was fitted with a ratio of

polynomials. This approach involved a system identification technique with system constants obtained by minimization of frequency response functions over the frequency range of interest. It is not possible to relate these system constants to the physical properties of the track system. In [13], an approach was used for vertical track dynamics based on a multi-degree of freedom (MDOF) mass-spring system. This paper extends this modal summation approach to study the rail dynamics in vertical, longitudinal, lateral and spin (rotation about vertical) directions. This is then applied to Huang's curve squeal model. The role of rail dynamics and different friction laws are then explored using this extended model.

2. Theoretical squeal model

A complete curve squeal model consists of several sub-models, which relate to vehicle dynamics, wheel/rail dynamics, contact dynamics, and acoustic radiation. The vehicle dynamics provides the necessary parameters related with the steady-state curving behaviour; time domain and frequency domain models for the wheel/rail system are developed by combining wheel/rail dynamics and contact dynamics; finally, an acoustic radiation model is used for predicting the sound pressure level from vibration.

In the frequency domain, the wheel and rail dynamics are described by their mobility matrices. The wheel mobility can be obtained by modal analysis after determining the modal parameters from a finite element analysis for the wheel. The rail mobility is obtained from an analytical model which will be summarised in Section 3. In the contact zone, only vertical contact spring is considered, thus the normal force fluctuates because of the compression or extension of the contact spring. The fluctuation of the normal force leads to fluctuations in the friction force which leads to an asymmetric matrix. This is the reason for possible mode coupling instability. Friction forces in lateral, longitudinal and spin direction are determined by using the FASTSIM algorithm [14]. By combining wheel dynamics, rail dynamics and contact dynamics, a self-excited vibration loop can be obtained (see Figure 1). If the contact friction forces $\mathbf{F^f}$ are applied, the sliding velocities matrix $\mathbf{V^s}$ can be obtained by using mobility matrix $\mathbf{G}$, which will then give a modified set of forces through a linearized frictional impedance matrix $\mathbf{H_1}$. Matrix $\mathbf{H_2}$ gives the linearized effect from the fluctuation of normal force on the friction forces. Thus, the stability can be studied using the open loop transfer function of the self-excited vibration loop, which is $(\mathbf{H_1 G + H_2})$ [11].

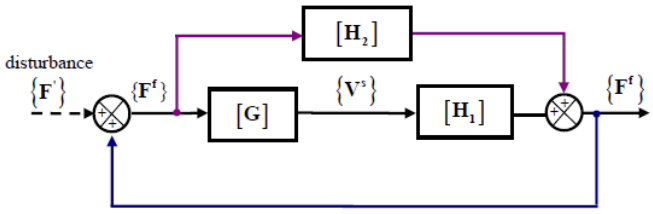

Figure 1. Linearized self-excited vibration loop of the wheel/rail contact system [11].

In the time domain, state-space models are used for the wheel and rail. The state-space rail model will be introduced in Section 3; the state-space wheel model can be developed by using a similar method once the modal parameters are obtained as above. If some small disturbances of the friction force are given, the wheel and rail will produce dynamic responses, which will in turn update the contact force and feed back to the wheel and rail system. Hence, step by step integration will be used to obtain the time history response of the wheel and rail.

3. Rail vibration

Analytical rail models have been developed by other researchers to give the point mobilities of the rail in different directions. The vertical vibration response has been presented by Grassie in [15] by using a beam on two-layer support model. Wu and Thompson [16] gave the lateral vibration response of railway track based on a multi-beam model. Lurcock [17] studied the longitudinal motion. Spin motion of the rail was modelled for squeal analyses using a Timoshenko beam model [11]. The stability analysis performed in the frequency domain makes direct use of these results. Cross mobilities are not considered in the present work.

3.1. Equivalent MDOF track model

These analytical rail models, however, are not suitable to the step-by step integration in the time domain. An equivalent track model is adopted instead which is based on a multi-degree of freedom mass-spring system (see Figure 2), a similar method has been used in [18] to study ballasted tracks. The application of the extra mode in Figure 2 will be explained below. According to the modal summation approach [19], for a MDOF system, the displacement at DoF j due to a force F_k at DoF k is:

$$X_{j,k} = F_k \sum_{i=1}^{n} \frac{\psi_i(j)\psi_i(k)}{-\omega^2 + \omega_i^2 + 2j\zeta_i\omega\omega_i} \tag{1}$$

where ω_i is the natural frequency of i^{th} mode, ω is the excitation frequency, ψ_i is the mass-normalised mode shape and ζ_i is the modal damping ratio. With this formulation, it is not necessary to derive the mass and stiffness of this system, because modal parameters are used instead.

The receptance from analytical models which are based on an infinite track shows peaks at the cut on frequencies of waves in the rail. According to the number of cut on frequencies in the frequency range considered, the number of modes included in the equivalent modal model can be defined. Their natural frequencies are chosen to be the same as the cut on frequencies in analytical model.

Take the vertical point receptance of the track for example. Figure 3 shows a comparison of the rail vertical receptance between the analytical model (solid line) and a modal model (dashed line). From the analytical model, it can be found that there are two peaks at 80Hz and 700Hz, which are also chosen as the natural frequencies in the modal model. It should be noticed that hysteretic damping, as used in the analytical model, cannot be used in a time-domain model. Hence, a viscous damping model is applied in the modal model, and according to [20], a suitable choice of viscous damping coefficient C is obtained by equating it to the required hysteretic damping value at the corresponding cut on frequency, i.e. $C = \frac{s\eta}{\omega_0}$, where s is the stiffness, η is the damping loss factor, ω_0 is the cut on frequency.

Moreover, it can be seen from Figure 3 that the analytical and modal models match well up to 1 kHz, but at higher frequencies the agreement is less good. This is because, for an infinite track, energy is carried away from the driving point at high frequency due to free wave propagation along the rail. Consequently the receptance of a Timoshenko beam tends to a phase of $-\pi/2$ and a slope of $1/\omega$ at high frequency whereas the modal model tends to a phase of $-\pi$ and a slope of $1/\omega^2$ equivalent to mass. In order to get a better match at high frequency, an additional spring/damper set with a small mass is included in series with the mass/spring model, see Figure 2. This can be considered as adding an extra mode to the system; its natural frequency is set equal to 20 kHz which is beyond the frequency range considered in the current study. Again, there is no need to know the mass associated with this extra mode. It can be seen that the modal model with extra mode (dotted line) gives a better fit with analytical model (solid line).

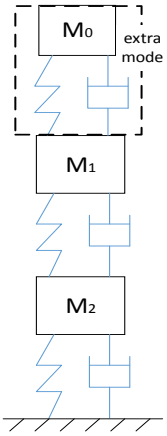

Figure 2. Modal model for track vertical receptance

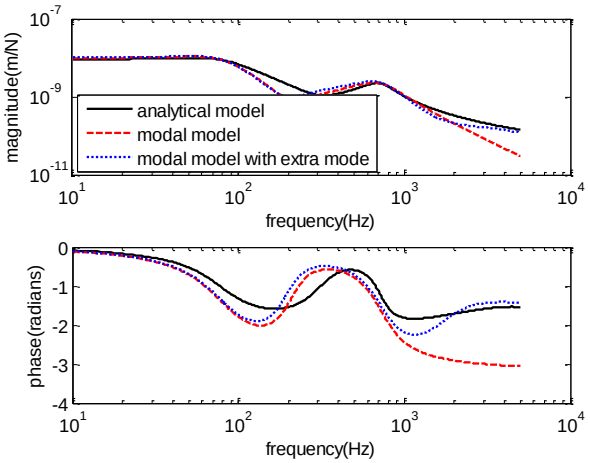

Figure 3. Comparison of track vertical receptance between analytical model and modal model

The results from the equivalent MDOF models for lateral and longitudinal directions are shown in Figure 4; these are obtained with the same method although in the lateral direction more modes are included. It should be mentioned that, for spin direction, the modal model cannot match the analytical results well, which needs to be solved in the future.

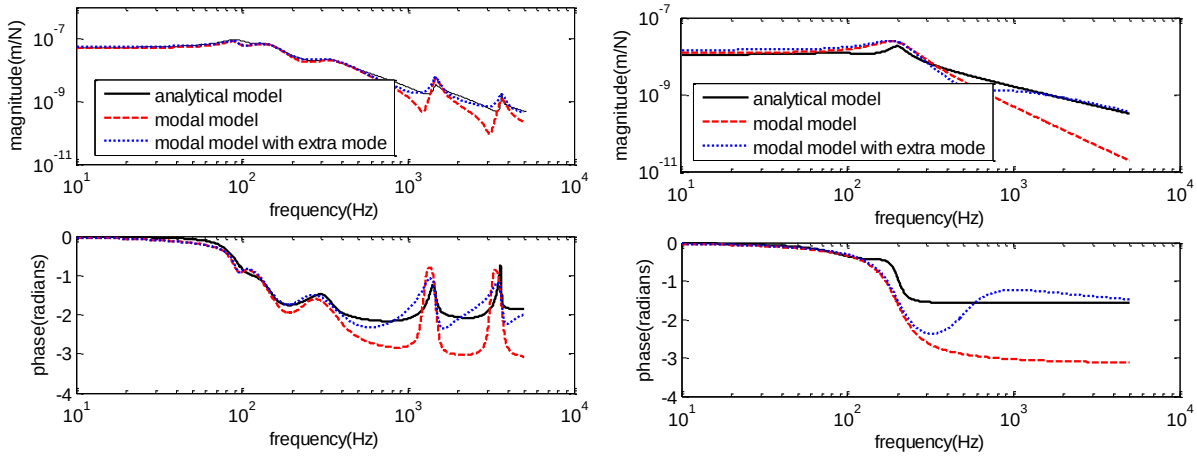

(a) lateral direction (b) longitudinal direction

Figure 4. Comparisons of track lateral and longitudinal receptance between analytical model and modal model

3.2. State-space matrix for track dynamics

A state-space model of the rail is required for the simulations in the time domain. After the equivalent mass-spring system has been built with the modal analysis method, the state-space model can be easily obtained for these mass-spring systems. Separate modal models are obtained for four directions: vertical, longitudinal, lateral and spin.

Consider a mass-spring system with *n* modes, one input dynamic force *f*, and output dynamic velocity on one direction $\{V^{\mathrm{r}}\} = [v_1^{\mathrm{r}}]$. This can be represented by a state equation and an output equation as:

$$\{\dot{R}\} = [A^{\mathrm{r}}]\{R\} + [B^{\mathrm{r}}]f \tag{2}$$

$$\{V^{\mathrm{r}}\} = [C^{\mathrm{r}}]\{R\} \tag{3}$$

where the state variable vector R consists of the modal velocity $\dot{q}_i$ and the modal displacement q_i of mode i (1 to n)

$$\{R\} = [\dot{q_1},\ \dot{q_2}, \ldots, \dot{q_n}, q_1, q_2, \ldots, q_n]^{\mathrm{T}} \tag{4}$$

The system matrix $[A^{\mathrm{r}}]$ is:

$$[A^{\mathrm{r}}] = \begin{bmatrix} -2\zeta_1\omega_1 & & & & -\omega_1^2 & & & \\ & -2\zeta_2\omega_2 & & & & -\omega_2^2 & & \\ & & \ddots & & & & \ddots & \\ & & & -2\zeta_n\omega_n & & & & -\omega_n^2 \\ 1 & & & & 0 & & \cdots & 0 \\ & 1 & & & & 0 & & \\ & & \ddots & & \vdots & & \ddots & \vdots \\ & & & 1 & 0 & & \cdots & 0 \end{bmatrix} \tag{5}$$

where ζ_i is the damping ratio of mode i and ω_i is the natural frequency (in radians/sec) of mode i. The input matrix $[B^{\mathrm{r}}]$ can transform external forces into modal forces for each mode, while the output matrix $[C^{\mathrm{r}}]$ sums modal velocities of each mode into external velocities. Both matrices are formed from the mode shapes, for example:

$$[B^{\mathrm{r}}] = [\phi_{11}\ \phi_{12}\ \cdots \phi_{1n} \mid 0, 0 \cdots 0\ ]^{\mathrm{T}} \tag{6}$$

and

$$[C^{\mathrm{r}}] = [\phi_{11}\ \phi_{12}\ \cdots \phi_{1n} \mid 0, 0 \cdots 0\ ] \tag{7}$$

where ϕ_{1i} is the mass-normalised modeshape of mode *i* in 1 direction.

By assembling the mass-spring state-space models for the four directions, the total system matrix $[A]$, input matrix $[B]$ and output matrix $[C]$ are given as follows:

$$[A] = \begin{bmatrix} [A_{11}^{\mathrm{r}}] & & & \\ & [A_{22}^{\mathrm{r}}] & & \\ & & [A_{33}^{\mathrm{r}}] & \\ & & & [A_{66}^{\mathrm{r}}] \end{bmatrix} \tag{8}$$

$$[B] = \begin{bmatrix} [B_{11}^{\mathrm{r}}] & & & \\ & [B_{22}^{\mathrm{r}}] & & \\ & & [B_{33}^{\mathrm{r}}] & \\ & & & [B_{66}^{\mathrm{r}}] \end{bmatrix} \tag{9}$$

$$[C] = \begin{bmatrix} [C_{11}^{\mathrm{r}}] & & & \\ & [C_{22}^{\mathrm{r}}] & & \\ & & [C_{33}^{\mathrm{r}}] & \\ & & & [C_{66}^{\mathrm{r}}] \end{bmatrix} \tag{10}$$

where the subscript 1 refers to the longitudinal direction, 2 to the lateral direction, 3 to the vertical direction and 6 to spin. Thus, the matrices $[A]$, $[B]$and $[C]$ can be obtained according to the parameter values obtained from curve fitting.

4. Friction law

The rolling friction force depends on the relative sliding velocity at the contact. For small sliding velocity, the friction force increases linearly from zero, until it saturates at the Coulomb friction limit. This is the adhesion zone where micro-slip occurs in part of the contact. After this zone, the rolling contact is under gross sliding. The friction law used in this paper is from Huang [11], which is based on Kalker's FASTSIM theory [14] together with a falling part, defined as:

$$\tau(\gamma) = 1 - \lambda e^{\kappa/|\gamma|} \tag{11}$$

where λ is the falling ratio, κ is the saturation coefficient, and γ is the creepage.

To study whether squeal can occur with a constant friction, a friction law without falling part is also considered. Therefore, both of the friction curves in Figure 5 will be employed to study the occurrence of squeal. Some important parameters for the friction curve are listed in Table 1.

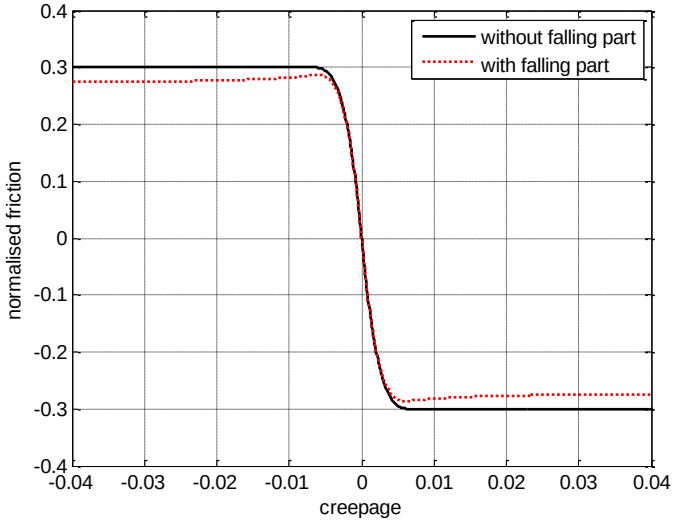

Figure 5. Two friction laws used in this paper

Table 1. Parameters used for friction force curves

Description and Name	Unit	Value
Coulomb friction coefficient μ_0	/	0.3
Falling ratio λ in Eq.(11)	/	0.1
Saturation coefficient κ in Eq.(11)	/	0.005
Longitudinal creepage	/	0
Spin creepage	/	0
Longitudinal semi-axis of contact ellipse a	mm	10
Lateral semi-axis of contact ellipse b	mm	5

5. Results

5.1. Parameters of cases studied

To study the role of rail dynamics and falling friction characteristics, four cases are calculated here, which are described in Table 2. Cases 1 and 2 are with falling friction; rail dynamics is included in Case 1 but not in Case 2. Meanwhile constant friction is adopted for Cases 3 and 4, again with and without the rail dynamics respectively. A wheel from a Class 158 multiple unit train [11] (see Figure 6) is used in all these cases. Some important parameters used in all these cases are shown in Table 3. In the present work, the contact angle is set as 2° and the contact is assumed to be located at the nominal wheel/rail contact point, which is not necessarily representative of a train running around a curve.

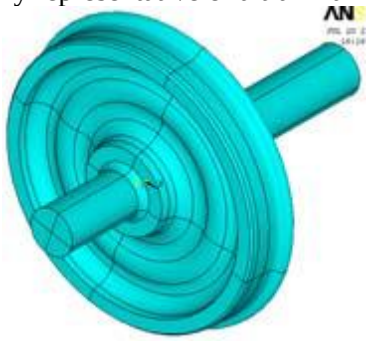

Figure 6. Solid model of Class 158 wheel

Table 2. Cases description

Case number	Falling friction (✓) or constant friction(✕)	Include rail(✓) or not (✕)
1	✓	✓
2	✓	✕
3	✕	✓
4	✕	✕

Table 3. Some input parameters and their values

Description and Name	Unit	Value
Normal force N	kN	60
Rolling velocity V_0	m/s	10
Lateral steady state creepage γ_2	/	0.02
Longitudinal steady state creepage γ_1	/	0
Spin steady state creepage γ_6	/	0

5.2. Frequency domain analysis

To study the stability of the wheel/rail system, a generalised Nyquist stability criterion is applied, which can be stated as follows. The system will be closed-loop stable if and only if the net sum of anti-clockwise encirclements of the critical point (-1/*k*, *j*0) by the set of eigenloci of the open-loop transfer function matrix (TFM) is equal to the total number of right-half plane poles of the TFM, where for negative feedback, k =1, and for a positive feedback, k = -1 [21]. In order to predict the possible unstable frequencies in the squeal loop, only the eigenvalue with maximum modulus at each frequency is chosen to judge the stability [11]. In addition, to have intuitive frequency information, the Bode plot is also employed.

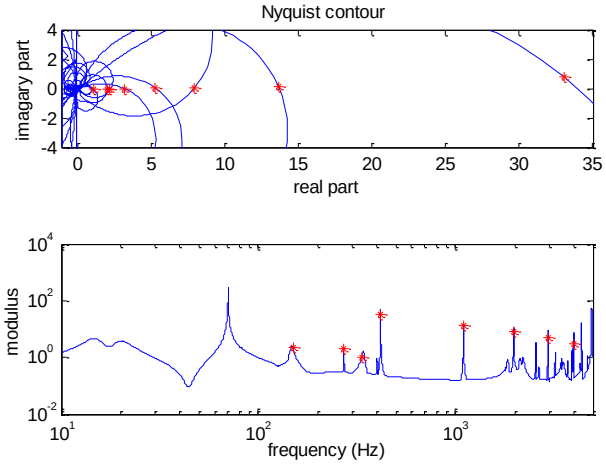

Figure 7. Case 1: Nyquist contour of eigenloci and modulus of the Bode diagram of eigenloci: * unstable frequencies

Figure 7 gives the stability analysis for Case 1. The unstable frequencies are shown in both Nyquist contour and the modulus graph of the Bode plot, which are marked by a '*'. The same thing has been done for Cases 2-4, all the useful results are summarised in Table 4. The wheel modes involved are identified by their natural frequencies (Hz) and their indices (*n*,*m*) in Table 4. The wheel modes listed as responsible for the corresponding unstable frequencies are verified by including only these wheel modes in the analysis to see whether the unstable frequencies remain. To describe the wheel modes, the number of nodal diameters *n* and the number of nodal circles *m* are used. The word 'axle' means an axle bending mode, the index '*r*' means a radial wheel mode, '*x*' means other modes.

Comparing the results of Cases 1 and 2 in Table 4, it can be seen that with a falling friction force, the frequency at 150.5Hz can be eliminated if the rail is not included in this model. However, the modulus at this unstable frequency is 2.131, which is much smaller than most of other unstable frequencies, meaning that this one is unlikely to be the dominant unstable frequency.

Comparing the results of Cases 3 and 4 shows that even with a constant friction force, the system can still be unstable at some frequencies. This indicates that falling friction is not the only reason for curve squeal instability. Interestingly, in Case 3, two wheel modes are coupled for the unstable frequency at 3974Hz, but for the unstable frequencies at 150.8Hz, 272.5Hz, 418.2Hz, 1102Hz and 1977Hz, only one single wheel mode is responsible for each unstable frequency, which means these instabilities do not come from the wheel mode coupling. When rail is not considered the number of unstable frequencies for constant friction reduces from 6 to 2, which means the existence of the rail can have a significant impact on the existence of squeal instability.

Table 4. Summary of frequency domain analysis for Cases 1-4

Case 1 (falling friction /rail included)	Unstable frequencies (Hz)	150.5	272.5	401.4	418.6	1102	1976	2951	3977
	Loop gain	2.131	6.753	1.556	14.2	7.997	6.373	4.728	2.858
	Wheel modes involved (Hz)	149.42	272.54	402.03	418.34	1102	1976.2	2950.4	3977.4
	(n,m)	(1,0)	(0,0)	(0,*x*)	(2,0)	(3,0)	(4,0)	(5,0)	(6,0)
Case 2 (falling friction/ rigid rail)	Unstable frequencies (Hz)		269.2	400.1	420.2	1103	1976	2951	3977
	Loop gain		2.755	1.811	35.89	16.87	6.523	5.091	2.647
	Wheel modes involved (Hz)		272.54	402.03	418.34	1102	1976.2	2950.4	3977.4
	(n,m)		(0,0)	(0,*x*)	(2,0)	(3,0)	(4,0)	(5,0)	(6,0)
Case 3 (constant friction /rail included)	Unstable frequencies (Hz)	150.8	272.5		418.2	1102	1977		3974
	Loop gain	2.01	6.348		8.722	6.613	3.153		1.234
	Wheel modes involved (Hz)	149.42	272.54		418.34	1102	1976.2		3915.1 3977.4
	(n,m)	(1,0)	(0,0)		(2,0)	(3,0)	(4,0)		(4,1) (6,0)
Case 4 (constant friction /rigid rail)	Unstable frequencies (Hz)		263.1				1977		
	Loop gain		1.543				2.913		
	Wheel modes involved (Hz)		82.37 149.42 272.54				1959.4 1976.2		
	(n,m)		(axle) (1,0) (0,0)				(2,*r*) (4,0)		

In order to study the detailed effect of rail dynamics on the mode coupling, some extended cases have been considered based on Case 3. It is found that the instabilities at 150.8Hz, 272.5Hz, 418.2Hz, 1102Hz and 1977Hz in Case 3 can be eliminated if the normal modal displacement of the wheel mode is set to 0, even though the rail is included. This means that the instabilities at these frequencies are not due to the coupling between wheel modes and rail dynamics; they are more likely to occur because of the coupling between the tangential component and normal component of the single wheel mode, when normal contact is included. Nevertheless the rail mobility can change the flexibility of the normal contact, which affects the degree of coupling.

It is also found that using a different wheel design can produce very different results. For instance, if a straight-webbed wheel is used and the contact angle is set to 0°, the system will always be stable under the same conditions as Case 3.

5.3. Time domain analysis

In the time domain, a step by step integration method is used including the state-space models for wheel and rail. The velocity time histories of wheel and rail in different directions can be obtained. To quantify the squeal noise level, an engineering method [22] is employed here to determine the sound pressure level (SPL) at 7.5 m from the sound source. Only the noise radiation from wheel is considered. Figure 8 to Figure 11 show the time history results and narrow-band velocity spectra for Cases 1-4. Figure 12 gives the A-weighted SPL of Cases 1-4.

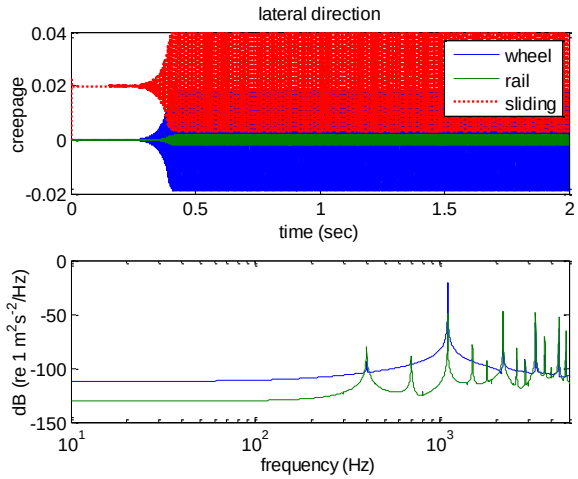

Figure 8. Time history of Case 1

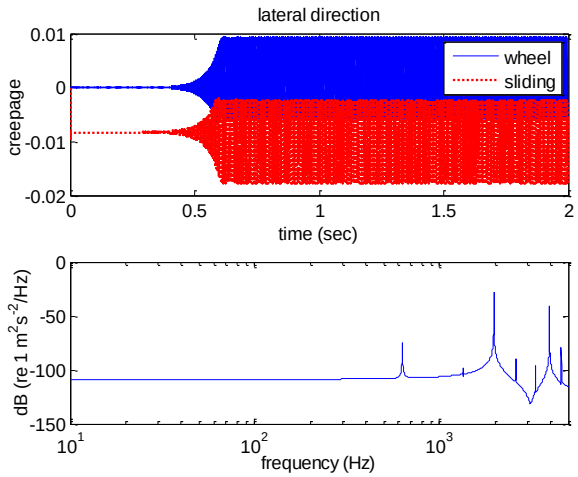

Figure 9. Time history of Case 2

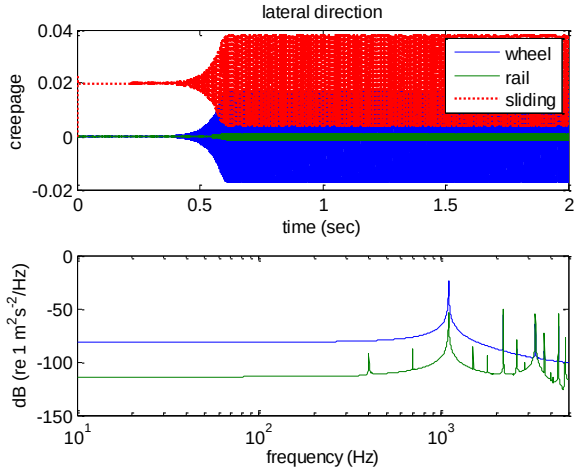

Figure 10. Time history of Case 3

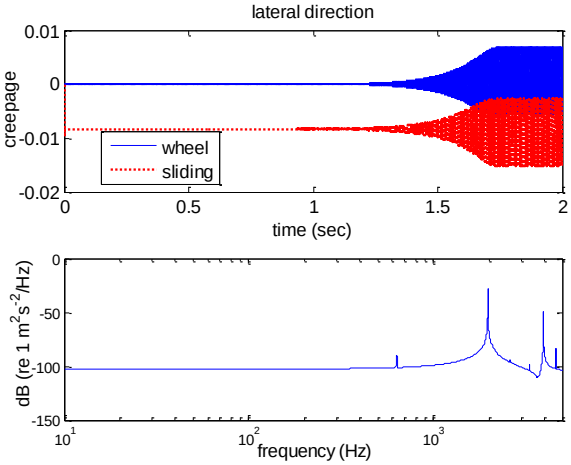

Figure 11. Time history of Case 4

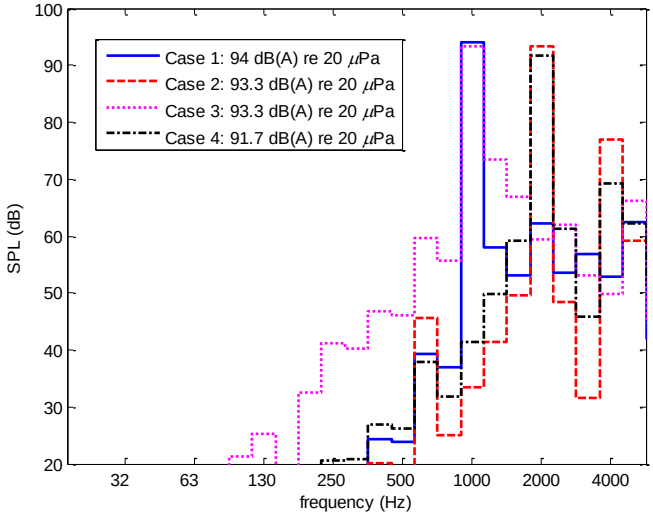

Figure 12. Noise radiation from the wheel

The time history results show that a steady state response is obtained for all four cases considered, which means squeal exists in all these cases. Moreover, it can be seen that the amplitude of vibration in the rail is much smaller than the response of the wheel. The spectra in Figure 8 and Figure 10 show that,

although a few possible unstable frequencies can be found in the frequency domain, only one becomes dominant in the time domain. For Case 1 and Case 3 this is at 1100 Hz. Other peaks exist in the response spectrum; some of them are higher harmonics of 1100 Hz (due to non-linearities) while others correspond to the rail modes. The wheel mostly vibrates sinusoidally at 1100 Hz showing the highest amplitude, but the rail spectrum can be greater than that of the wheel at the higher harmonics or at the frequencies of the rail modes. Figure 9 and Figure 11 show that the dominant frequency changes to 1978 Hz when the rail is neglected.

Each of the two dominant frequencies found for the cases with and without rail (1100 and 1978 Hz) corresponds with one of those found in the frequency domain analysis in Table 4, although they are not necessarily the ones with the largest loop gain.

For these examples, the total sound pressure levels for Cases 1 to 4 are quite similar (Figure 12).

6. Conclusions

A systematic study has been presented to show the effect of rail dynamics and friction condition on squeal noise. By performing the stability analysis, it is found that, while a falling characteristic of the friction force generally leads to curve squeal, it is not the only reason for the squeal. Wheel mode coupling or even the coupling between the tangential component and normal component of the single wheel mode can also be responsible in some situations. Rail dynamics is found to play an important role when constant friction is considered. Time history results show that squeal instability exists even with a constant friction force, and the presence of the rail can change the dominant frequency of squeal noise.

7. References

[1] Rudd M 1976 Wheel/rail noise—Part II: Wheel squeal *J Sound Vib* **46** 381-94
[2] Fingberg U 1990 A model of wheel-rail squealing noise *J Sound Vib* **143** 365-77
[3] Heckl M A and Abrahams I D 2000 Curve Squeal of Train Wheels, Part 1: Mathematical Model for Its Generation *J Sound Vib* **229** 669-93
[4] Périard F 1998 Wheel-Rail Noise Generation: Curve Squealing by Trams. Technische Universiteit Delft)
[5] Chiello O, Ayasse J B, Vincent N and Koch J R 2006 Curve squeal of urban rolling stock—Part 3: Theoretical model *J Sound Vib* **293** 710-27
[6] Brunel J F, Dufrénoy P, Naït M, Muñoz J L and Demilly F 2006 Transient models for curve squeal noise *J Sound Vib* **293** 758-65
[7] Xie G, Allen P, Iwnicki S D, Alonso A, Thompson D J, Jones C J C and Huang Z 2006 Introduction of falling friction coefficients into curving calculations for studying curve squeal noise *Vehicle Syst Dyn* **44** 261-71
[8] Hoffmann N, Fischer M, Allgaier R and Gaul L 2002 A minimal model for studying properties of the mode-coupling type instability in friction induced oscillations *Mech Res Commun* **29** 197-205
[9] Glocker C, Cataldi-Spinola E and Leine R 2009 Curve squealing of trains: Measurement, modelling and simulation *J Sound Vib* **324** 365-86
[10] Pieringer A 2014 A numerical investigation of curve squeal in the case of constant wheel/rail friction *J Sound Vib* **333** 4295-313
[11] Huang Z 2007 Theoretical Modelling of Railway Curve Squeal. (UK: University of Southampton)
[12] Wu T and Thompson D J 2000 Theoretical investigation of wheel/rail non-linear interaction due to roughness excitation *Vehicle Syst Dyn* **34** 261-82
[13] Yang J 2012 Time domain models of wheel/rail interaction taking account of surface defects. University of Southampton)
[14] Kalker J 1982 A fast algorithm for the simplified theory of rolling contact *Vehicle Syst Dyn* **11** 1-13
[15] Grassie S, Gregory R, Harrison D and Johnson K 1982 The dynamic response of railway track to high frequency vertical excitation *J Mech Eng Sci* **24** 77-90

[16] Wu T and Thompson D J 1999 Analysis of lateral vibration behavior of railway track at high frequencies using a continuously supported multiple beam model *J Acoust Soc Am* **106** 1369-76
[17] Lurcock D E J 2004 An investigation into the longitudinal vibration properties of railway track. In: *ISVR*: University of Southampton)
[18] Gerstberger U, Knothe K and Wu Y 2003 *System Dynamics and Long-Term Behaviour of Railway Vehicles, Track and Subgrade*: Springer) pp 247-64
[19] Ewins D J 1995 *Modal testing: theory and practice* vol 6: Research studies press Letchworth)
[20] Thompson D J 2009 *Railway Noise and Vibration: Mechanisms, Modelling and Means of Control*: Elsevier: Oxford)
[21] Barmanj J F and Katzenelson J 1974 A generalized Nyquist-type stability criterion for multivariable feedback systems *Int J Control* **20** 593-622
[22] Thompson D J and Jones C J C 2002 Sound radiation from a vibrating railway wheel *J Sound Vib* **253** 401-19